Electronic Supplementary Information

Particle Size-Dependent Viscoelastic Fe(II)-Triazole Composites in the Low-Spin State.

M. Kermarrec,[a,b] C. J. Gómez-García,[c] M. Marchivie,[d] P. Roquefort,[b] T. Aubry,[b] and S. Triki[a]

[a]*Univ Brest, CNRS, CEMCA, 6 Avenue V. Le Gorgeu, C.S. 93837 - 29238 Brest, France*

[b]*Univ Brest,* CNRS, IRDL, *6 Avenue V. Le Gorgeu, C.S. 93837 - 29238 Brest, France*

[c]*Departamento de Química Inorgánica, Universidad de Valencia, C/Dr. Moliner 50, 46100 Burjasot (Valencia) Spain.*

[d]*CNRS, Univ. Bordeaux, Bordeaux, 87 Avenue du Dr A. Schweitzer, 33608 Pessac, France.*

Chemicals

All chemicals were acquired from Sigma-Aldrich (MERCK): Iron(II) tetrafluoroborate hexahydrate ($Fe(BF_4)_2 \cdot 6H_2O$), 1,2,4-triazole (Htrz), sodium polystyrene sulfonate (NaPSS, $M_{av} = 10^6$ g.mol^{-1}). The reagent used for the nanoparticles synthesis **A1** and **A2** are: dioctyl sulfosuccinate sodium salt (AOT), n-Octane (reagent grade, 98%). The syntheses and composite elaboration were carried out with ultra-pure water (18 MΩ.cm).

Synthesis

Particles **A1** (32 nm), **A2** (65 nm) and **C** (1.2 µm) have been prepared according to the reported procedure,[1-2] while **B** (474 nm) particles have been synthesized using the following original procedure: An aqueous solution (6 mL) of sodium polystyrene sulfonate (1.202 g, 5.8 mmol) containing iron(II) tetrafluoroborate hexahydrate (0.984 g, 2.9 mmol) was stirred at

room temperature for two hours. Then, the clear solution was heated to 80 ºC and the ligand 1,2,4-triazole (0.605 g, 8.7 mmol), previously grinded into a fine powder, was slowly added to the polymer solution, under constant stirring. After one hour at 80 ºC, heating was stopped while stirring was maintained at room temperature for 20 hours. Then the solution was centrifuged (30 min, 11 000 rpm, 20 ºC) to separate particles from the polymer. The collected pink powder was washed three times with 20 mL of pure water. The product was dried and kept under argon atmosphere to prevent iron oxidation. From the elemental analysis (see Table S1) the chemical formula was determined: $[Fe(Htrz)_2(trz)](BF_4)\cdot H_2O\cdot(NaPSS)_{0.16}$ (M = 399.84 $g.mol^{-1}$, yield = 0.554 mg = 48 %). Elemental analyses were performed for all $[Fe(Htrz)_2(trz)](BF_4)$ particles to quantify the surfactant impurities (Table S1). For the four composites, C, H, N and S content was determined with a Thermofisher flashmart analyzer. Two measurements for each element were performed (Table S2). Fe was analyzed using ICP-Mass spectrometry performed with an Agilent Technologies spectrometer (ICP-MS model 7900) spectrometer. The samples were dissolved in acid with the help of a microwave oven (Table S3).

Table S1. Elemental analyses of $[Fe(Htrz)_2(trz)](BF_4)$ particles.

		C (%)	H (%)	N (%)	S (%)
A1	Found	31.8	3.9	24.6	2.2
	Calculated for $[Fe(Htrz)_2(trz)](BF_4)\cdot(AOT)_{0.36}$	31.2	4.2	24.8	2.3
A2	Found	24.6	3.1	31.5	0.9
	Calculated for $[Fe(Htrz)_2(trz)](BF_4)\cdot(AOT)_{0.11}$	24.8	3.1	31.7	0.9
B	Found	22.7	2.7	31.5	1.3
	Calculated for $[Fe(Htrz)_2(trz)](BF_4)\cdot H_2O\cdot(NaPSS)_{0.16}$	21.9	2.8	31.5	1.3
C	Found	19.5	2.6	34.0	-
	Calculated for $[Fe(Htrz)_2(trz)](BF_4)\cdot H_2O$	19.6	2.7	34.4	-

Table S2. Elemental analyses of $[Fe(Htrz)_2(trz)](BF_4)$/NaPSS composites.

		C (%)	H (%)	N (%)	S (%)
A1/NaPSS	Found	32.5	4.0	10.6	8.4
	Calculated for $[Fe(Htrz)_2(trz)](BF_4)\cdot 7H_2O\cdot(AOT)_{0.36}$/2.1NaPSS*	33.7	4.7	11.8	7.4
A2/NaPSS	Found	29.1	3.4	13.3	7.9
	Calculated for $[Fe(Htrz)_2(trz)](BF_4)\cdot 7H_2O\cdot(AOT)_{0.11}$/2NaPSS	31.0	4.3	13.5	7.2
B/NaPSS	Found	29.1	3.2	13.8	7.8
	Calculated for $[Fe(Htrz)_2(trz)](BF_4)\cdot 7H_2O$/2.1NaPSS*	30.2	4.1	13.9	7.4
C/NaPSS	Found	28.1	3.0	15.5	7.1

	Calculated for $[Fe(Htrz)_2(trz)](BF_4)\cdot 6H_2O/2NaPSS$	30.4	3.9	14.5	7.4

Table S3. Iron content in $[Fe(Htrz)_2(trz)](BF_4)$/NaPSS composites, determined by ICP-MS.

		Fe (%)
A1/NaPSS	Found	5.6
	Calculated for $[Fe(Htrz)_2(trz)](BF_4)\cdot(AOT)_{0.36}$/2.1NaPSS*	5.9
A2/NaPSS	Found	7.1
	Calculated for $[Fe(Htrz)_2(trz)](BF_4)\cdot(AOT)_{0.11}$/2NaPSS	6.9
B/NaPSS	Found	7.1
	Calculated for $[Fe(Htrz)_2(trz)](BF_4)$/2.1NaPSS*	7.1
C/NaPSS	Found	7.3
	Calculated for $[Fe(Htrz)_2(trz)](BF_4)$/2NaPSS	7.3

***Tables S2 and S3.** The **B/NaPSS** and **A1/NaPSS** composites exhibit a slightly higher NaPSS content compared to the other two composites (**C/NaPSS** and **A2/NaPSS**), despite identical amounts of NaPSS being used during their synthesis. As far as the **B/NaPSS** composite is concerned, the higher NaPSS content arises from the preparation of **B** nanoparticles in the presence of NaPSS polymer because of nanoparticles retaining traces of NaPSS, as confirmed by elemental analysis (see Table S1). In the case of the **A1/NaPSS** composite, the use of the surfactant AOT during synthesis contributes to the increase of NaPSS portion. Indeed, despite purification steps, complete removal of AOT was not achievable, as corroborated by the elemental analysis of the **A1** nanoparticles (see Table S1).

Infrared spectra

Infrared (IR) spectra were performed on the four synthesized particle samples (see Fig. S1-S4). All spectra exhibit an absorption band around 632 cm^{-1} corresponding to the triazole cycle in a C_{2v} symmetry, suggesting the bridging coordination mode N_1,N_2 of the triazole ring, whereas the triazolate (trz^-) ligand (C_{2v} symmetry) is likely responsible for the absorption band around 679 cm^{-1}. These bands are in good agreement with the formation of polynuclear chains, composed of triply bridged metal ions.[1] Both, **A1** and **A2** particles spectra exhibit two weak absorption bands around 1720 and 1640 cm^{-1}, corresponding to the ester stretching ν(C=O) of the sodium docusate surfactant used in the nanoparticle synthesis,[2] whose IR spectrum was also recorded for the sake of comparison (Fig. S5). Finally, it should be noted that the spectrum of **B** particles does not show any characteristic band of the NaPSS (Fig. S6).

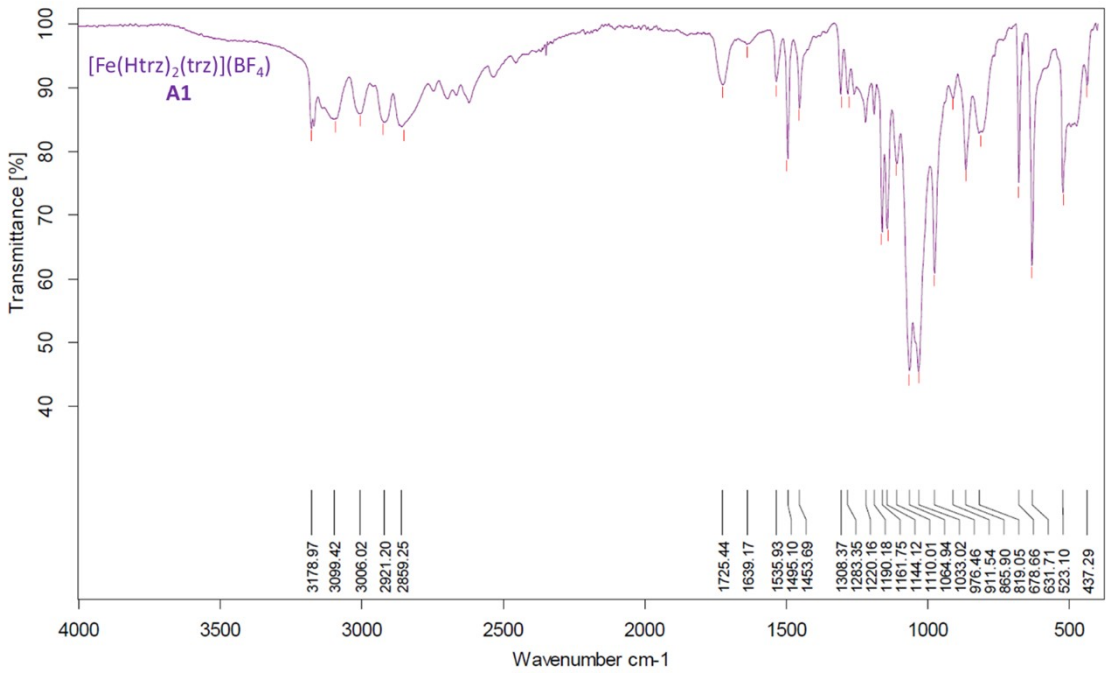

Fig. **S1**. Infrared spectrum of $[Fe(Htrz)_2(trz)](BF_4)$ **A1** particles (cm^{-1}): 3179w, 3099m, 3006m, 2921m, 2859m-br, *1725m, 1639vw*, 1536s, 1495s-sh, 1454s, 1308s, 1283m, 1190m, 1162s, 1144s, 1110w, 1065vs-br, 1033vs-br, 976w, 911w, 866s, 825m, 679vs-sh, 632vs-sh, 523s, 437w.

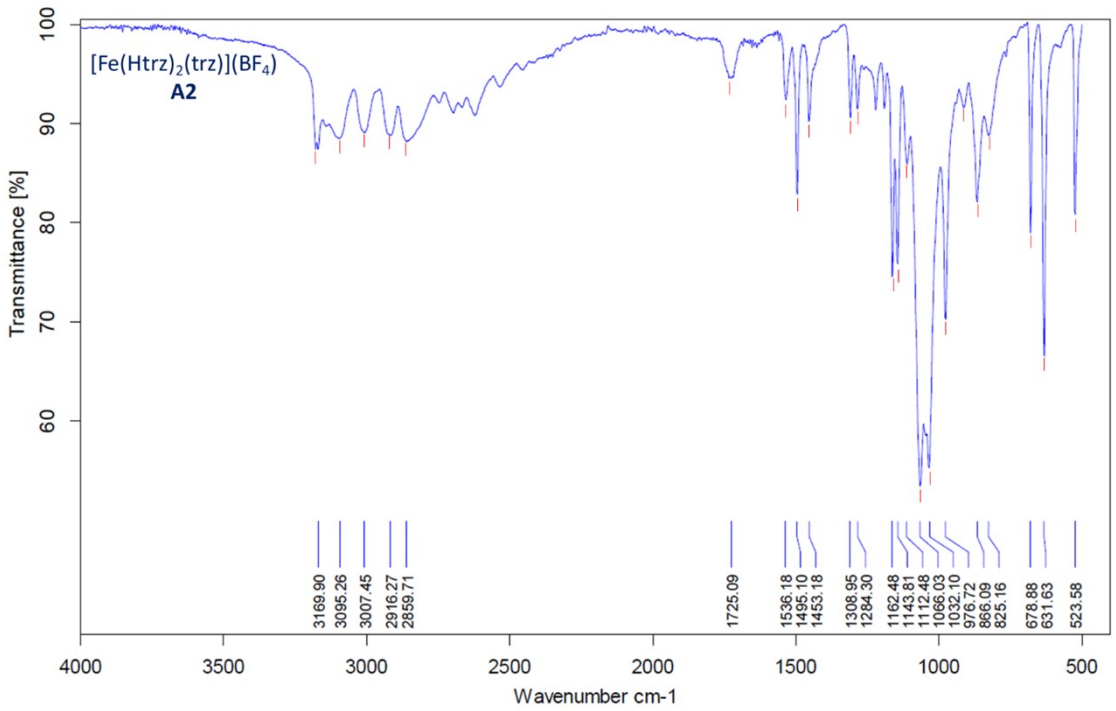

Fig. **S2**. Infrared spectrum of $[Fe(Htrz)_2(trz)](BF_4)$ **A2** particles (cm^{-1}): 3170w, 3095m, 3007m, 2916m, 2860m-br, *1725m*, 1536s, 1495s, 1453s, 1309s, 1284m, 1162s, 1144s, 1112w, 1066vs-br, 1032vs-br, 977w, 866s, 825m, 679vs-sh, 632vs-sh, 524vs-sh.

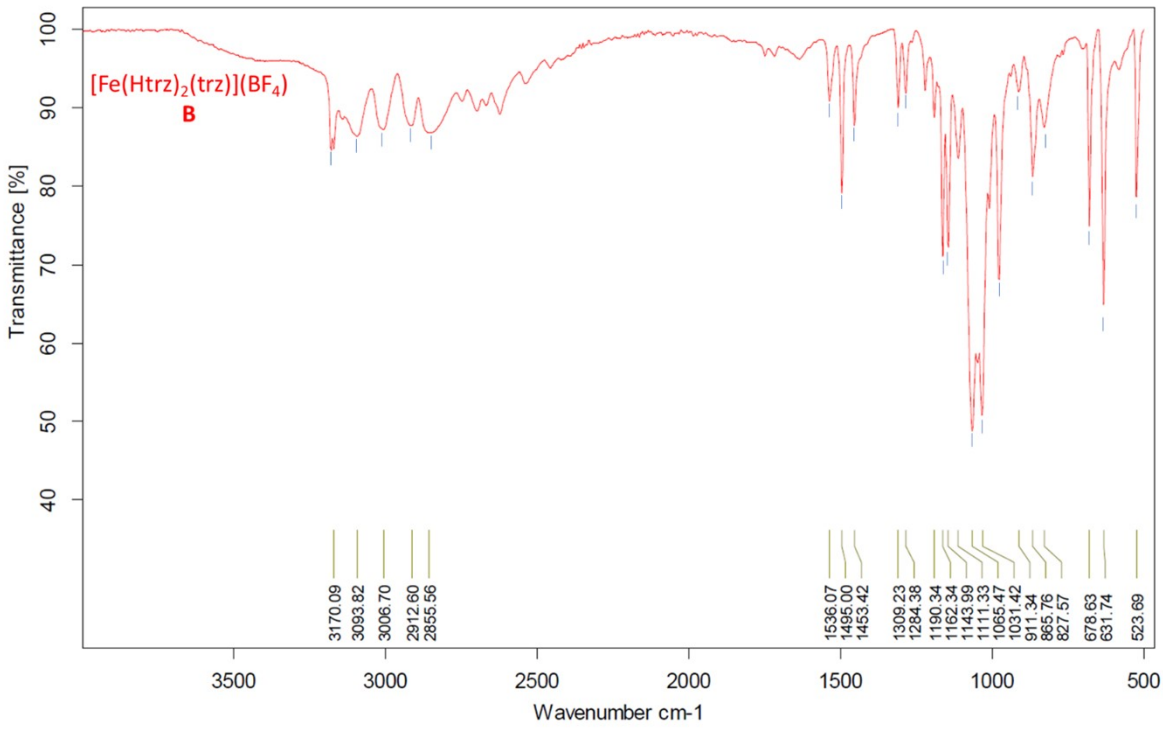

Fig. **S3**. Infrared spectrum of $[Fe(Htrz)_2(trz)](BF_4)$ **B** particles (cm^{-1}): 3170w, 3094m, 3007m, 2913m, 2856m-br, 1536s, 1495s, 1453s, 1309s, 1284m, 1190w, 1162vs, 1144vs, 1111w, 1065vs-br, 1031vs-br, 911w, 866s, 828m, 679vs-sh, 632vs-sh, 524vs-sh.

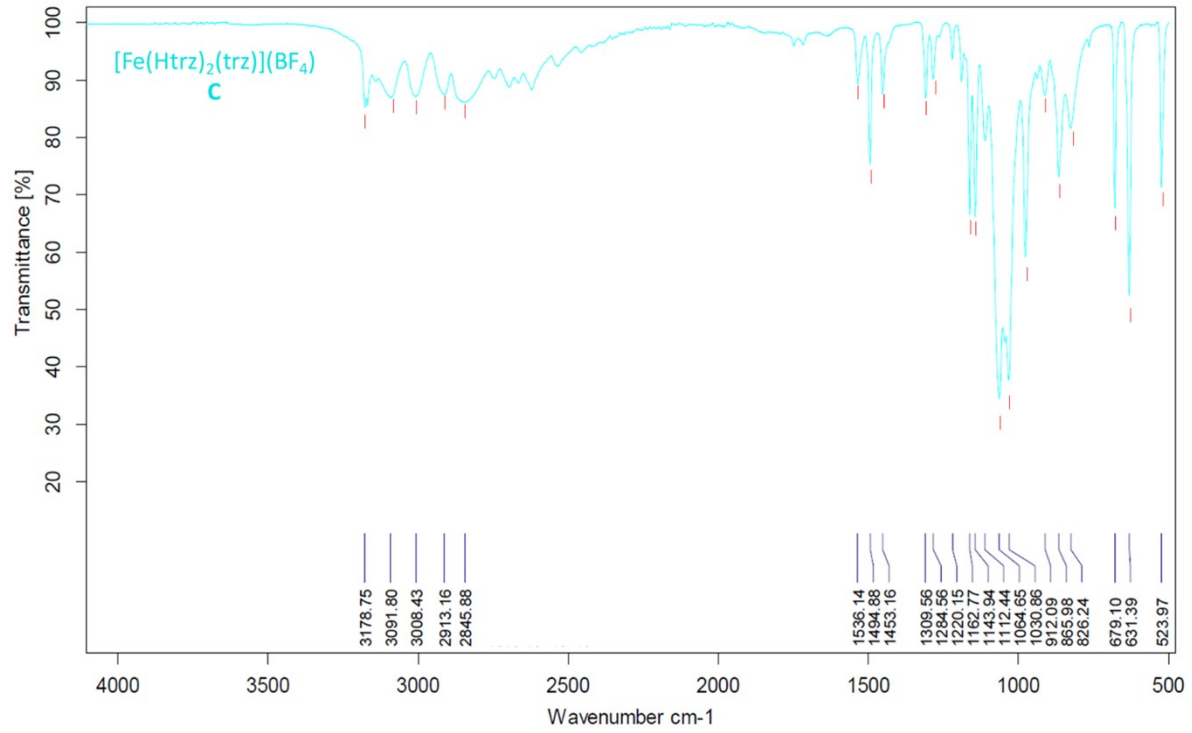

Fig. **S4**. Infrared spectrum of $[Fe(Htrz)_2(trz)](BF_4)$ **C** particles (cm^{-1}): 3179w, 3092m, 3008m, 2913m, 2846m-br, 1536s, 1495s, 1453s, 1310s, 1285m, 1220w, 1163vs, 1144vs, 1112w, 1065vs-br, 1031vs-br, 912w, 866s, 826m, 679vs-sh, 631vs-sh, 524vs-sh.

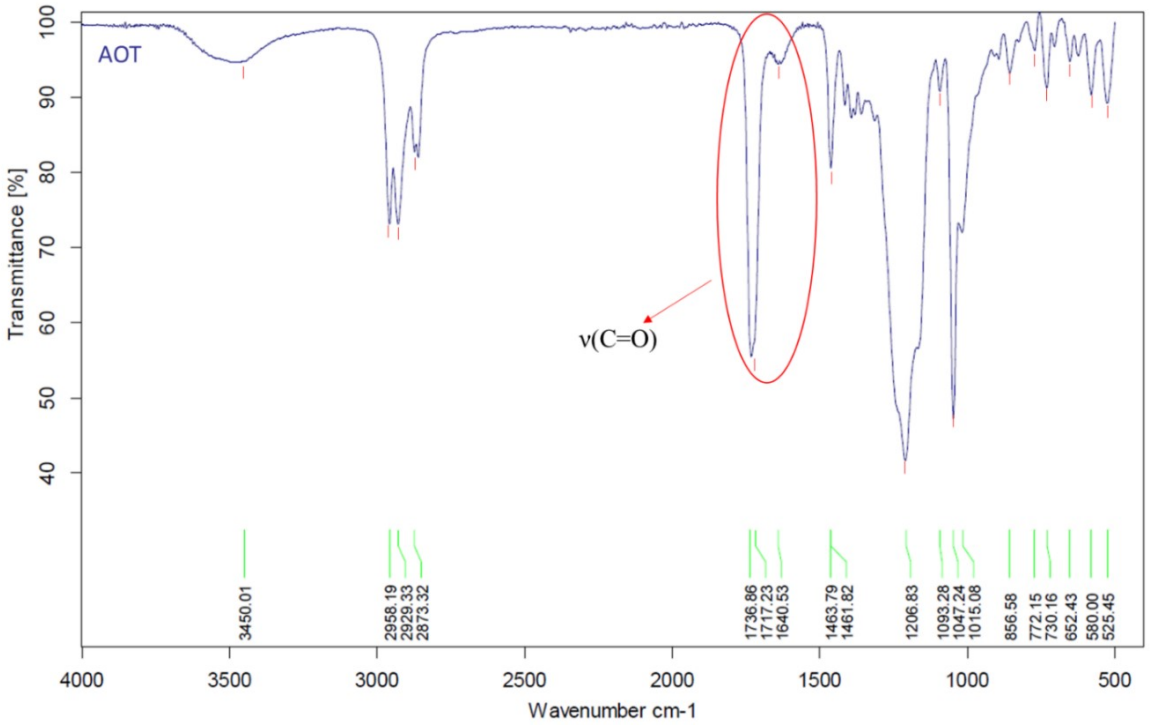

Fig. **S5**. Infrared spectrum of sodium docusate surfactant (cm^{-1}): 3450w-vbr(ν(H2O)), 2958s-br, 2929s-br, 2873s-br, 1717vs, 1640w, 1464m, 1207vs-br, 1093w, 1047vs, 1015w, 857w, 772w, 730m, 652w, 580m, 525m.

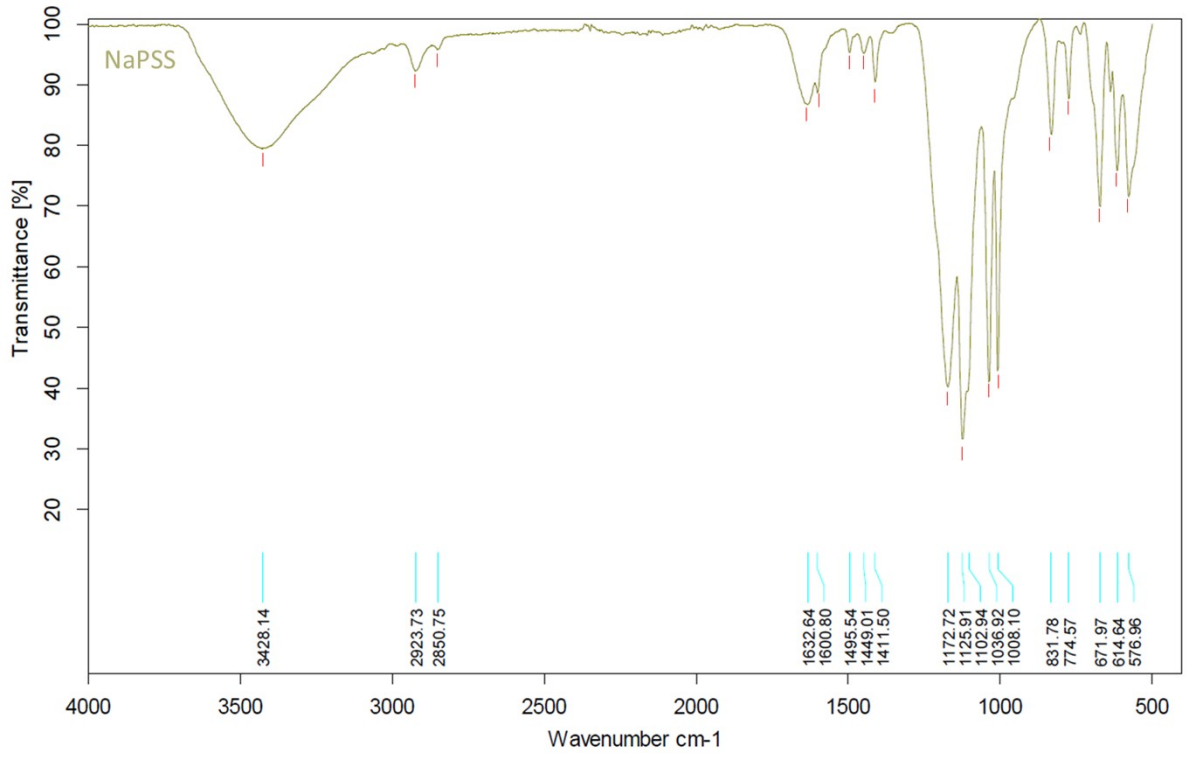

Fig. **S6**. Infrared spectrum of sodium polystyrene sulfonate polymer (cm^{-1}): 3428s-vbr(ν(H_2O)), 2924w, 2851vw, 1633m-br, 1495w, 1449w, 1411m, 1173vw-br, 1126vs-br, 1037vs, 1008vs, 832s, 775m, 672vs, 615s, 577s-br.

Thermogravimetric analysis

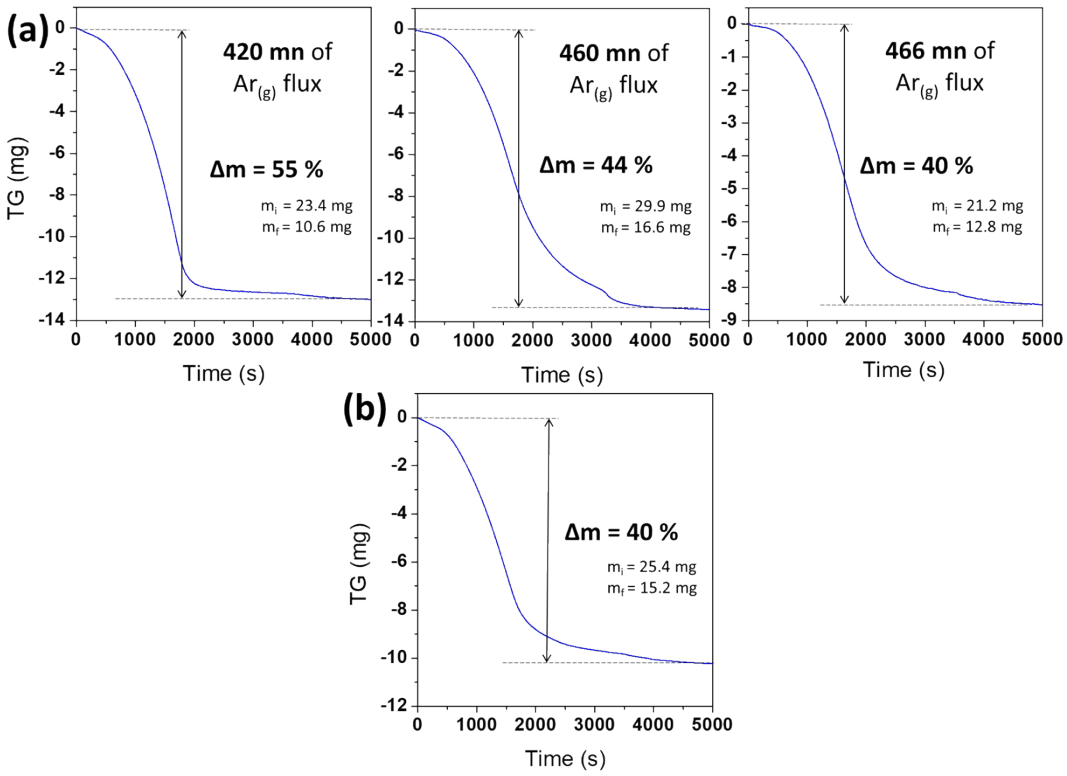

Fig. **S7**. (a) Thermogravimetric analysis (TGA) monitoring the evaporation of the **A1**/NaPSS composite under an argon flux; (b) final TGA curve for **A2**/NaPSS.

Microscopy

Particle geometry

The length (L), width (W) and aspect ratio (L/W) distributions of the different particles (Fig. S8, S9 and S10) can be correctly fitted using a log-normal distribution law,[3] characterized by the probability density function f (X; μ, σ):

$$f(X;\mu,\sigma) = \frac{A}{X\sigma\sqrt{2\pi}} e^{-\frac{(\ln(X)-\mu)^2}{2\sigma^2}}$$

Where A is a distribution normalizing constant, μ the mean value and σ the standard deviation of the nanoparticles dimension X (X: length, width, height or aspect ratio).

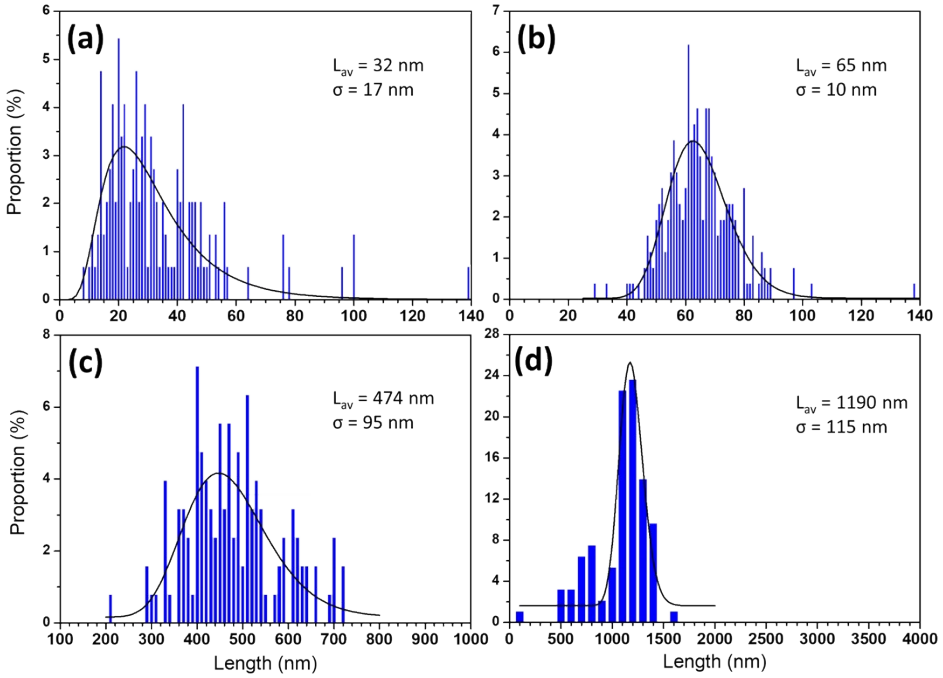

Fig. S8. Experimental values (columns) and fit with log-normal law (solid lines) of the length distribution for (a) **A1**, (b) **A2**, (c) **B** and (d) **C** particles. Insets show the average lengths (L_{av}) and standard deviations (σ).

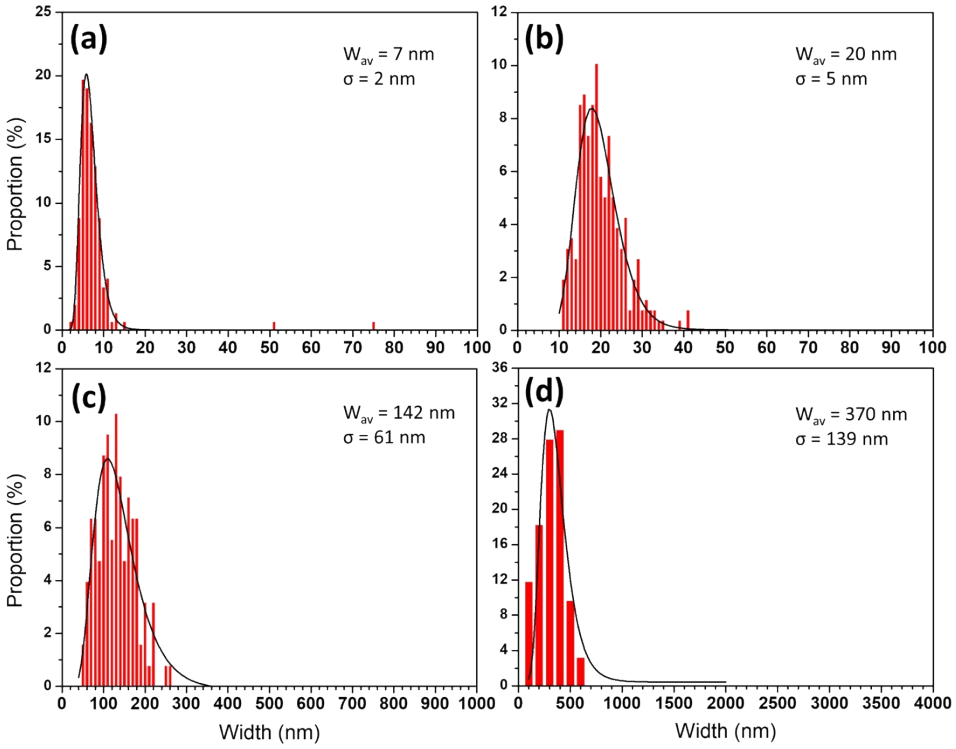

Fig. S9. Experimental values (columns) and fit with log-normal law (solid lines) of the width distribution for (a) **A1**, (b) **A2**, (c) **B** and (d) **C** particles. Insets show the average widths (W_{av}) and standard deviations (σ).

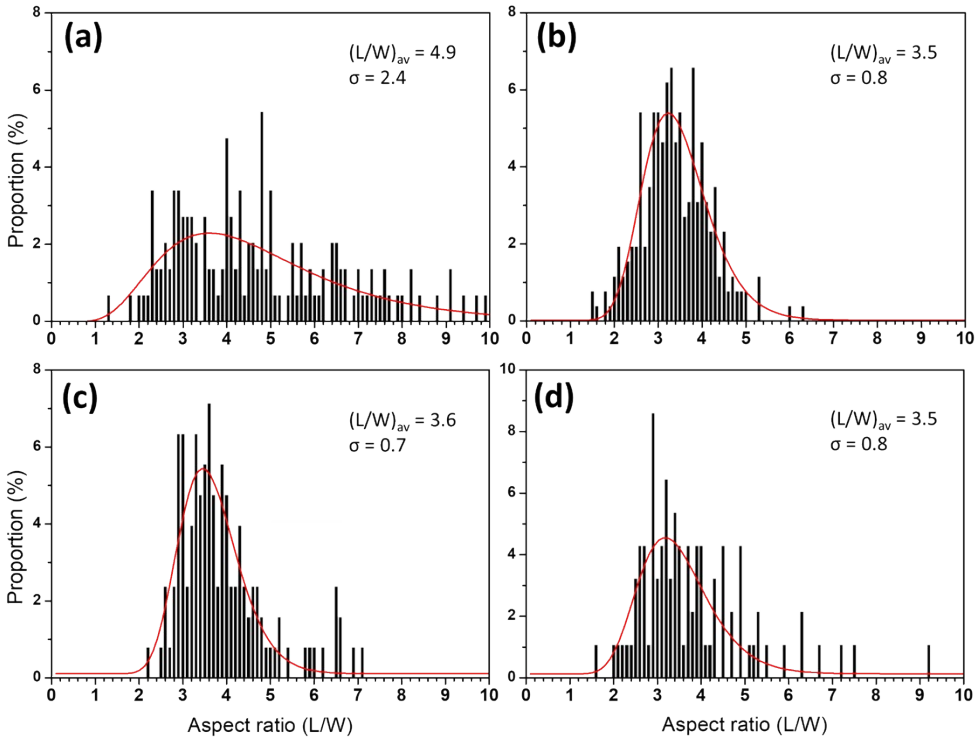

Fig. S10. Experimental values (columns) and fit with log-normal law (solid lines) of the aspect ratio (L/W) distribution for (a) **A1**, (b) **A2**, (c) **B** and (d) **C** particles. Insets show the average aspect ratio ($(L/W)_{av}$) and standard deviations (σ).

Sample preparation

Prior to TEM observations, $[Fe(Htrz)_2(trz)](BF_4)$ particles were dispersed in a water/ethanol mixture and sonicated for two minutes. Then, this suspension was drop casted on a copper grid (200 mesh = 75 µm) covered by a thin layer (5-6 nm) of carbon TEM-CF200CU5. For confocal observation, a drop of the composite **C**/NaPSS (1.2 µm) was placed in a 35 mm ibidi imaging µ-Dish borosilicate glass bottom. The glass part of the dish is 21 mm in diameter and 170±5 µm thick. The µ-Dish can be sealed with a lid during observation, in order to prevent the sample from drying out. The composite drop observed in confocal was slowly dried under normal conditions. The resulting half-sphere was cryo-fractured, and the resulting surface was vacuum-metallized to allow investigation by scanning electron microscopy of the particle dispersion within the composite.

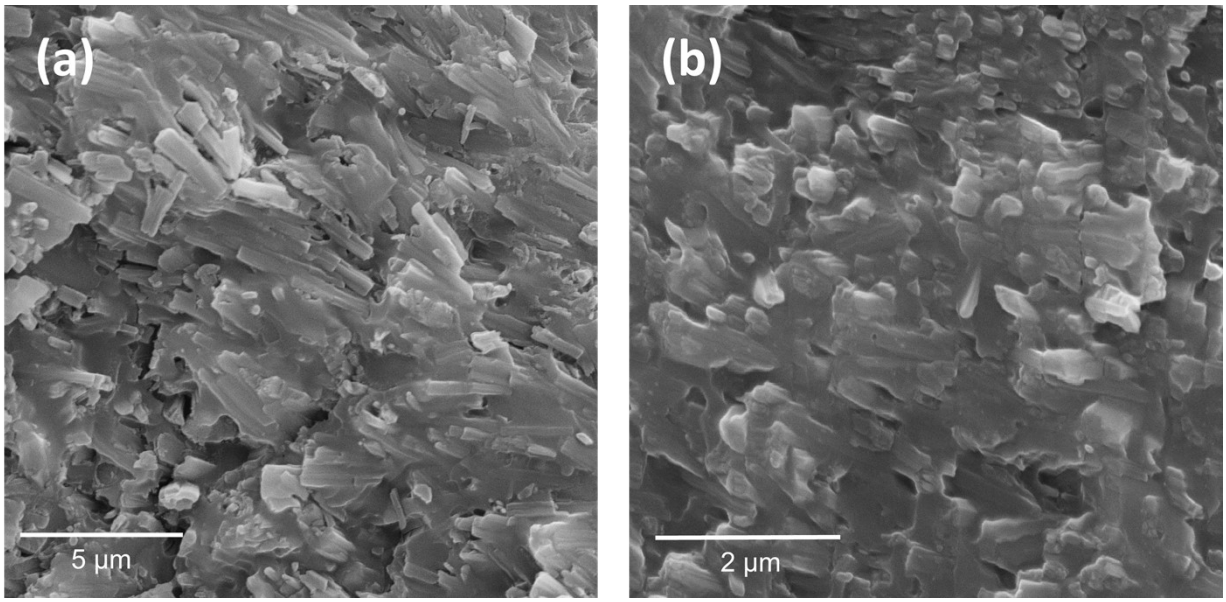

Fig. S11 Scanning electron microscopy (SEM) images of the composites (a) **C**/NaPSS and (b) **B**/NaPSS.

X-ray powder diffraction

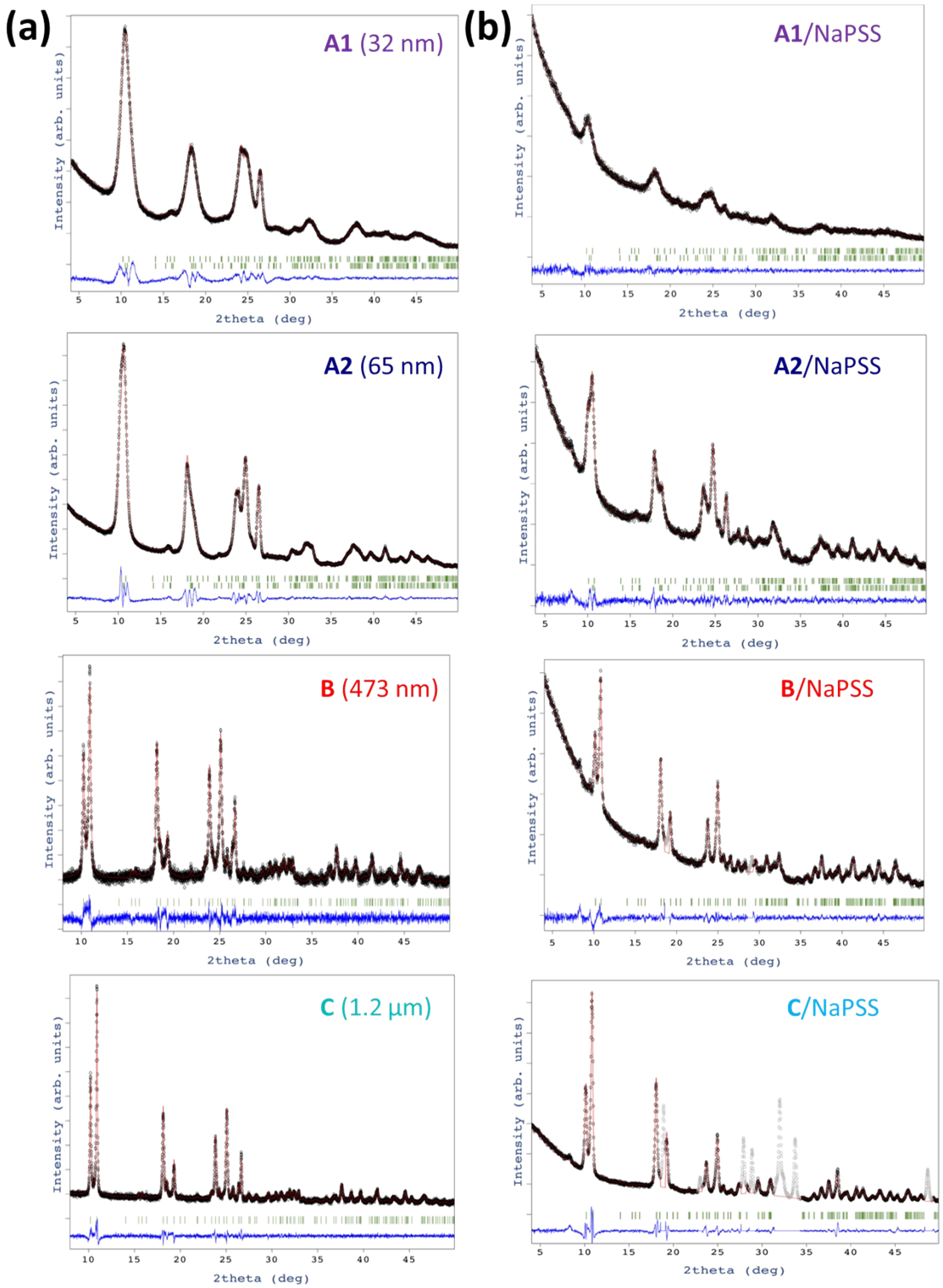

Fig. S12. X-Ray powder patterns of (a) $[Fe(Htrz)_2(trz)](BF_4)$ particles and (b) composites; black circles are experimental data, red continuous line is the calculated pattern from Rietveld

refinement, blue continuous line is the difference curve and green lines correspond to the Bragg peak positions.

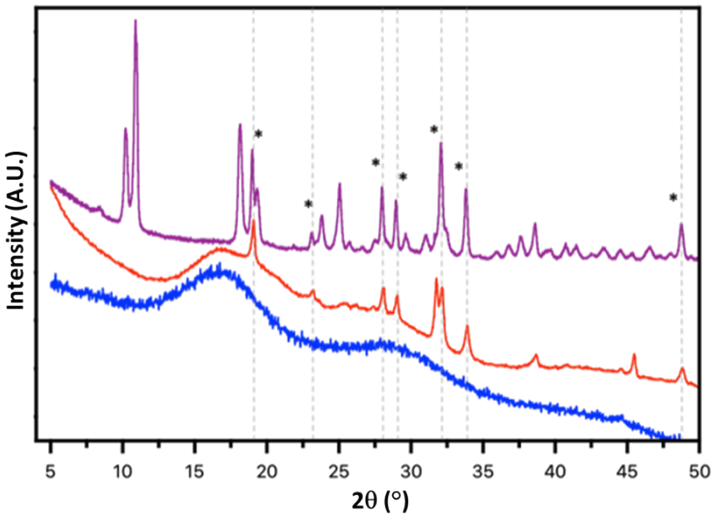

Fig. S13. X-Ray powder patterns of dehydrated NaPSS (red), dehydrated **C**/NaPSS composite (purple) and hydrated NaPSS (blue). Asterisks indicate non-indexed peaks in the **C**/NaPSS pattern. Grey dashed lines are guides for the eyes, showing the correspondence with the NaPSS peaks.

Rheology

For all the samples, the critical strain (γ_c), which characterizes the extent of the linear viscoelastic regime, was determined from the G', G" versus strain amplitude curves as the lowest strain amplitude corresponding to a 5 % relative decrease of the linear G' and G" plateau values, as shown in Fig. S14 for the NaPSS matrix.

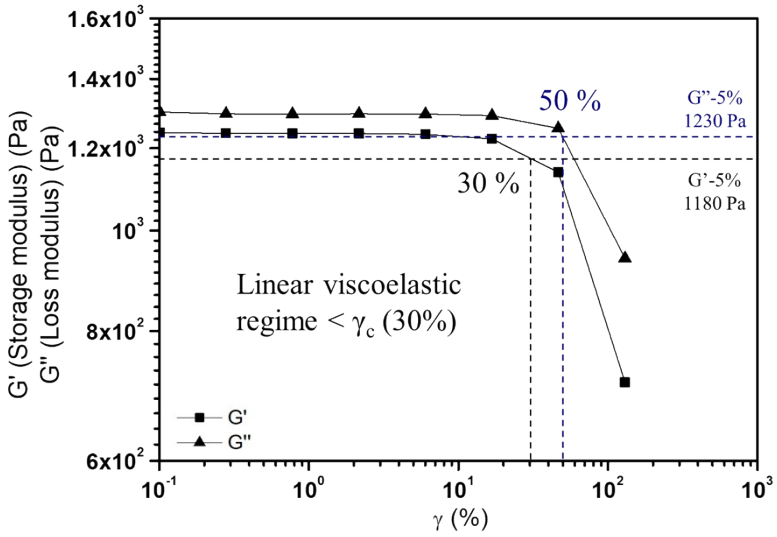

Fig. S14. Storage G' and loss G" moduli versus strain (γ) amplitude for a 4.85 M NaPSS aqueous solution (angular frequency: ω = 6.28 rad.s^{-1}).

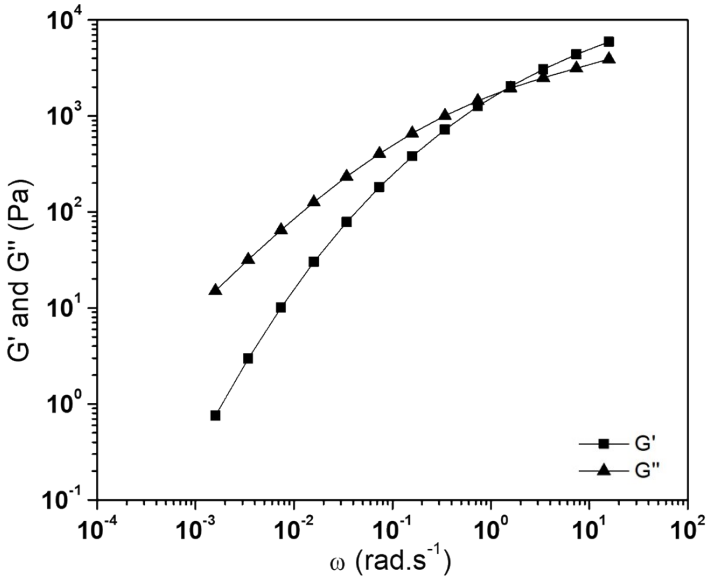

Fig. S15. Storage G' and loss G" moduli versus angular frequency ω, in the linear domain, for a 4.85 M NaPSS aqueous solution.

References

1 J. G. Haasnoot, G. Vos, W. L. Groeneveld, *Z. Naturforsch. B*, **1977**, *32*, 1421–1430.

2 M. Giménez-Marqués, M. L. García-Sanz de Larrea, E. Coronado, *J. Mater. Chem. C*, **2015**, *3*, 7946-7953.

3 I. Usov, G. Nyström, J. Adamcik, S. Handschin, C. Schütz, A. Fall, L. Bergström, R. Mezzenga, *Nat. Commun.,* **2015**, *6*, 7564.